Spatiotemporal profile of yoked superfluorescence from Rb vapor in the strong-excitation regime

Kenta Kitano* and Haruka Maeda
Department of Physics and Mathematics, Aoyama Gakuin University, Kanagawa, 252-5258, Japan

(Received 24 May 2018; published 22 June 2018)

We investigated both spatial and temporal profiles of the 420-nm yoked superfluorescence (YSF) from the atomic vapor of rubidium by driving the $5S-5D$ two-photon transition with an ultrashort laser pulse. By increasing the pump-pulse power beyond the saturation intensity, the spatial profile of the 420-nm YSF periodically changed between a central bright spot and a ring-shaped radial profile. The temporal profile of the 420-nm YSF was measured with a sampling oscilloscope with a time resolution of 50 ps. The experimental results were successfully reproduced by simulations using the Maxwell-Bloch equations. The simulated results confirmed that, in the strong excitation regime, the 420-nm emission from the lower transition component of the YSF is significantly delayed with respect to the 5.2-μm emission from the upper transition, while they are overlapped in the weak excitation regime.

DOI: 10.1103/PhysRevA.97.063418

I. INTRODUCTION

When a large number of two-level atoms are initially inverted without any coherence, a subsequent and spontaneous radiative decay process can build up a macroscopic dipole moment in the ensemble. The macroscopic dipole moment reaches its maximum at the superradiant state, where each atom is expressed as a superposition of the upper and lower states with equal populations. More importantly, each atomic dipole oscillates in phase due to the mutual coupling given by the common radiation field. This cooperative behavior of the atoms can result in the emission of a short coherent burst called superfluorescence (SF). Since the first discussion of the underlying physics of SF by Dicke in 1954 [1], several experimental and theoretical reports have revealed many of its fundamental features; these include the scaling laws of the peak intensity, the SF pulse width and delay time on the total number of excited atoms [2], and the ringing properties as well as the transverse coupling effect [3]. The early experiments were performed on various gas media [4] and molecular ions in crystals [5], while the more recent studies have been extended to a variety of physical systems, such as He atoms [6], electron-hole pairs in semiconductors [7] and in nanostructures [8], and Fe nuclei in solids [9]. The temporal profiles of SF pulses can be analyzed by a semiclassical treatment using the Maxwell-Bloch equations, in which the spatiotemporal field evolution is initiated by a fluctuating polarization or a field source in place of the quantum-mechanical noise [10].

Compared to the extensive studies on SF in two-level systems, there are only few reports about the same phenomenon in a cascade three-level system. Ikeda *et al.* analyzed this problem for the first time by preparing the atoms with a coherent superposition of upper and lower states in a three-level system [11]. They predicted that if the SF is emitted by the upper transition within the decoherence time of the system, it simultaneously induces the lower transition, while at the same time, the lower transition prevents the coherence to grow between the upper and middle states, delaying the upper SF. This coherent interplay between the two transitions was experimentally demonstrated by Brownell *et al.* and is called the yoked SF (YSF)[12]. As seen above, the temporal behavior of YSF is not a simple succession of SF in a two-level system. In addition, the beam emitted in the YSF has characteristic features. The upper SF is radiated into a relatively broad solid angle determined by a sample geometry, as happens in conventional SF. On the other hand, the lower SF is combined only with the narrow component of the upper SF that satisfies the phase-matching condition, resulting in a highly directional emission. This was successfully demonstrated by Lvovsky *et al.* by means of noncollinear double-pulse excitations [13]. In this sense, YSF is considered as a time-delayed four-wave mixing (FWM) process.

Several studies have been carried out to understand and control YSF [14–19]. However, in most cases, YSF has been analyzed under the following two assumptions. The first one is that the atoms are initially prepared in the weak excitation regime, although YSF shows a complex behavior in the strong excitation regime [13,14] and, in certain cases, the lower SF shows a ring-shaped beam profile [17]. The second one is that the YSF evolves in a linear regime [11,12], where the populations of the atomic states stay unchanged during the development of YSF, but this assumption is not suitable to quantitatively describe the YSF behavior, especially in a high-gain system. A detailed analysis beyond these two assumptions would deepen the understanding of YSF and, more importantly, enable its control, which is crucial for its applications in remote sensing [16] or for the development of new light sources. Based on the above considerations, we investigated the spatiotemporal characteristics of the YSF emitted by a dense atomic sample prepared in the strong excitation regime. The experimental results were quantitatively analyzed by simulations using a time-dependent Schrödinger equation as well as the Maxwell-Bloch equations with realistic parameters.

This paper is organized as follows. Section II describes the experimental details. Section III presents the experimental results. Section IV describes the calculation details. Section V

*kkitano@phys.aoyama.ac.jp

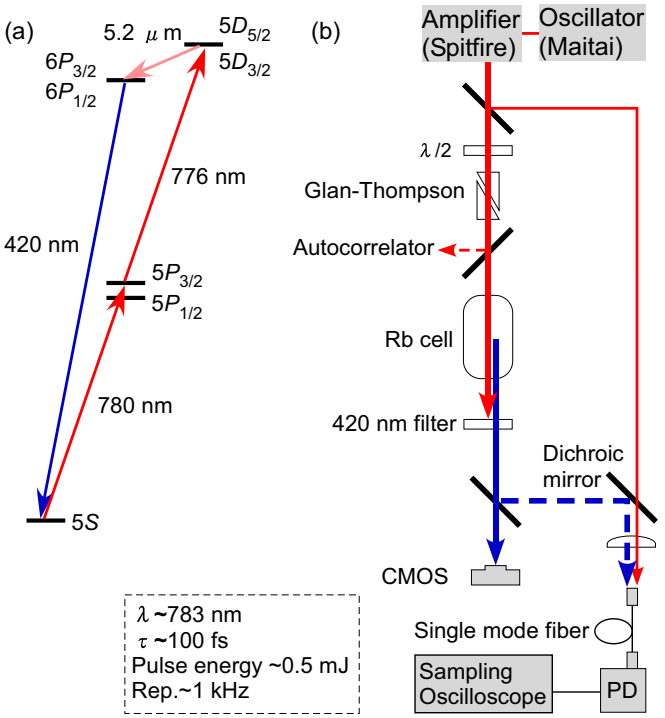

FIG. 1. (a) Energy diagram of Rb and the related transitions. (b) Schematic of the experimental setup.

provides the simulated results as well as the discussions. Conclusions and future perspectives are given in Sec. VI.

II. EXPERIMENTAL DETAILS

We first describe the atomic configuration and the radiation fields associated with the YSF of rubidium (Rb) atoms [see Fig. 1(a)]. The atoms are excited from the $5S$ ground state to the $5D$ excited state by a two-photon absorption induced with a femtosecond laser pulse, producing a coherent superposition of the upper, lower, and intermediate $5P$ states. After the pump pulse, a macroscopic coherence is developed in the medium, resulting in a SF emission on the $5D-6P$ transition, which in turn stimulates the $6P-5S$ transition due to the initially prepared $5S-5D$ coherence. The upper and lower transitions emit radiations with wavelengths of 5.2 μm (infrared) and 420 nm (blue light), respectively. In the present experiment, only the blue-light emission was observed.

A schematic of the experimental setup is shown in Fig. 1(b). We used a 100-fs Ti:sapphire laser system with a central wavelength of 783 nm, a repetition rate of 1 kHz, and a maximum pulse energy of 0.5 mJ. Although the central wavelength was detuned from the 778-nm two-photon resonant wavelength [see Fig. 1(a)], the $5S-5D$ transition still occurred due to the broad spectral width of the laser pulse, whose full width at half-maximum (FWHM) was 10 nm. In this work, this pulse was up-chirped to $\sim$310 fs from its transform limit of 100 fs by controlling the distance between paired gratings in the compressor. The pulse width was measured with a commercial autocorrelator. The horizontally polarized output beam was divided into two by a beam sampler (Thorlabs BSF10-B). The beam containing almost all the pulse energy was used as a pump pulse to excite the Rb atoms. The other beam worked as a time-reference pulse in the measurement of the temporal profiles of the blue-light emission. The pump-pulse power was varied by a half-wave plate combined with a Glan-Thompson polarizer. The pump beam was collimated with a telescope, which is not shown in Fig. 1(b), and entered a Pyrex-glass cell with a diameter of 2 cm and a length of 6 cm containing Rb vapor. The temperature of the cell was changeable in the range 170–200 °C. The beam profile of the pump pulse, which was measured with a complementary metal-oxide semiconductor (CMOS) camera (Thorlabs DCC1645C), was slightly elliptical having FWHMs of 1.20 mm and 1.26 mm in the horizontal and vertical directions, respectively. The blue light generated inside the cell was emitted almost collinearly with the pump beam. A bandpass filter (Thorlabs FB420-10) was placed behind the cell to block and transmit 45% of the blue-light power. The spatial profile of the transmitted blue light was monitored with the CMOS camera. To measure the temporal profile, the blue light and the time-reference pulse were both focused into a single-mode fiber (SMF) coupled with a 25 GHz high-speed photodetector (Newport 1434). The detector signal was recorded with a sampling oscilloscope (Tektronix SD-26).

III. EXPERIMENTAL RESULTS

When Rb atoms are strongly exited by intense ultrashort laser pulses, the spatial profile of the blue light dramatically changes depending on the pump-pulse intensity and chirp rate. In a recent work, we reported a ring-shaped radial profile for such blue-light beam[17]. In the present experiment, a periodic behavior of the spatial profile dependent on the pump-pulse intensity was demonstrated and the temporal profiles were also recorded to discuss the time evolution of YSF. The spatial profiles of the blue light recorded at 10 cm from the cell center at different pump-pulse powers (49 mW, 122 mW, 177 mW, and 272 mW) are shown in the upper row of Fig. 2(a). The temperature of the cell is fixed at 170 °C. With the gradual increase of the pump-pulse power, the blue light first appeared as a bright spot at the pump-beam center (A), then changed into a ring-shaped radial profile (B) with the radius increasing accordingly to input power. By further increasing the input power, the bright spot appeared again (C) to successively evolve in a similar way (D). At the input power of B, a clear double-ring structure and a weak outer ring were observed. Next, the spatial profiles were recorded by changing the distance from the cell center along the beam propagation axis; the results at different distances for the pump-pulse power values of A, C, and D are shown in Fig. 2(b). In the A case, the FWHM in the horizontal direction was 170 μm at 10 cm and 370 μm at 50 cm, from which the beam divergence was calculated as $\sim$0.5 mrad. Taking into account that the blue light is generated via a FWM process[13], its divergence is expected to be $\sim$0.6 mrad for the 6-cm sample cell, which is in agreement with the observed results. In the C case, the beam propagated similarly to A, although the two-photon excitations were clearly beyond saturation. In the D case, the ring radius remained almost unchanged along the propagation axis, but its width broadened due to the beam divergence. These results strongly suggest that the spatial profiles of the blue light were influenced by the nonlinear response of the Rb atoms

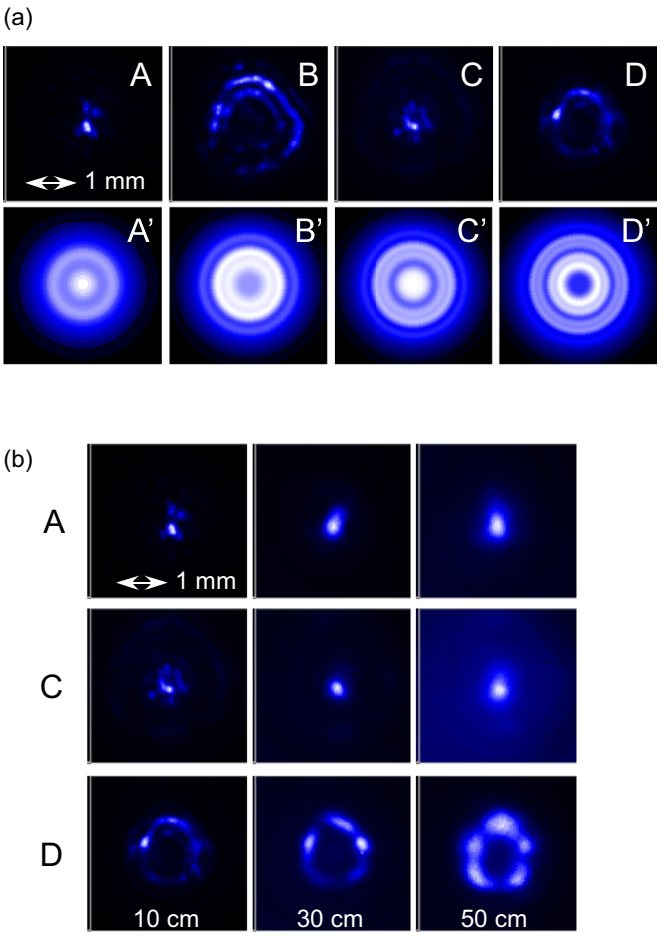

FIG. 2. (a) Experimental (upper row) and simulated (lower row) blue-light profiles at different pump-pulse conditions. A–D were recorded at pump-pulse power of 49 mW, 122 mW, 166 mW, and 272 mW, respectively. A′-D′ were simulated at the pump-pulse intensities indicated in Fig. 4(b). (b) Experimental blue-light profiles recorded at different distances from the cell center, indicated in the bottom panel of each column, at the pump-pulse power values of A, C, and D as in (a).

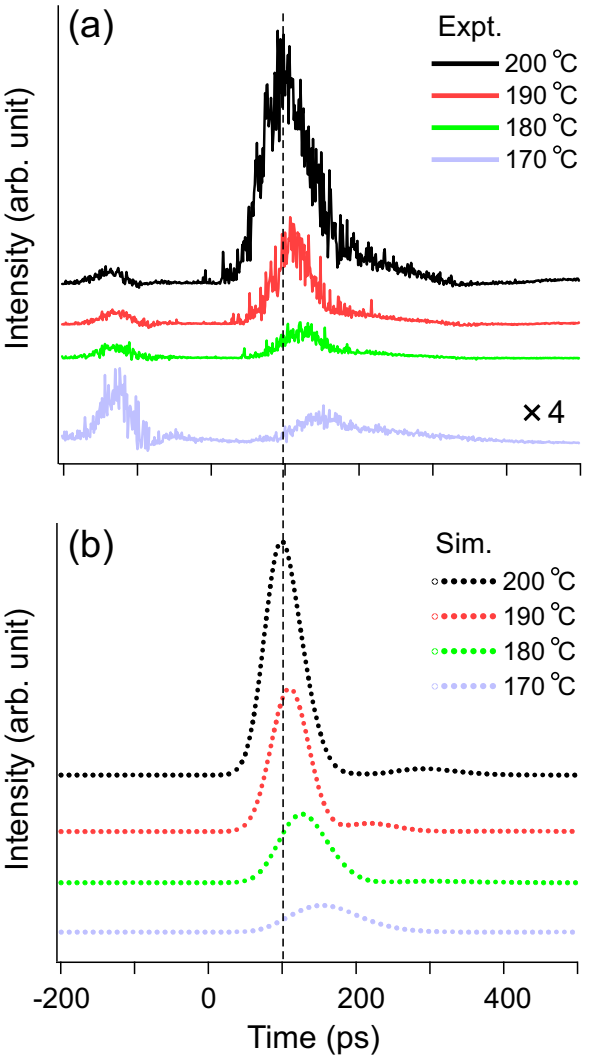

FIG. 3. Temporal profiles of the blue light at different temperatures. (a) Experimental results at the pump-pulse power in the C case of Fig. 2. (b) Simulated results at the pump-pulse intensity of 74 GW/cm^2.

to the pump field, without any beam focusing effect due to the propagation in a nonlinear medium, such as the Kerr lens effect. We also measured the blue-light power for the A case, which was ∼90 nW for the central bright spot. This value is compared with the simulated results in the later section.

Next, we measured the temporal profile of the blue light. To effectively couple the blue light to the SMF, its spatial profile is desirable to be a Gaussian profile. Therefore, we recorded the temporal profiles for the A and C cases. The temperature of the cell was scanned in the 170–200 °C range. Figure 3(a) shows the results for C, and similar ones were obtained for A. In addition to the blue light, the reference pulse was always monitored, and it can be seen at around −130 ps in the figure. This enabled us to evaluate the relative delay of the blue-light emission with respect to the pump pulse by eliminating a jitter of the laser system, although the absolute delay could not be measured due to the difference in the optical path lengths. The FWHM of the reference pulse was ∼50 ps, which indicates the time resolution of the detection system. The peak intensity of the blue light was larger and the relative delay smaller at the higher temperature. At 170 °C, the peak of the blue light was delayed of ∼40 ps with respect to that at 200 °C.

IV. CALCULATION DETAILS

To understand the spatial and temporal characteristics of the blue light obtained in the previous section, we performed numerical simulations that were divided into two parts. In the first part, we calculated the time evolution of a Rb electronic wave function under pump-pulse irradiation by solving a time-dependent Schrödinger equation for a single atom, including five states in total: $5S$, $5P_{3/2}$, $5P_{1/2}$, $5D_{5/2}$, and $5D_{3/2}$ [see Fig. 1(a)] [17]. We treated the radiation interaction in the dipole approximation, and the dipole matrix elements were represented as a product of Wigner 3-j symbol and a reduced matrix element [20,21], for which we used the values given in Ref. [22]. We chose a quantization axis along the polarization direction of the pump pulse so that

the magnetic quantum number of m_J remained unchanged according to the selection rule of $\Delta m_J = 0$. In the second part, we calculated the radiation decay process by solving the semiclassical Maxwell-Bloch equations, including five states in total: $5S$, $6P_{3/2}$, $6P_{1/2}$, $5D_{5/2}$, and $5D_{3/2}$. We applied a plane wave approximation and neglected the backward propagating wave. Then the Hamiltonian of the system in the interaction picture can be written in a retarded frame, $t \to t - z/c$, as follows [14,18,23]:

$$\frac{\hat{V}(t)}{\hbar} = \sum_{J=\frac{1}{2},\frac{3}{2}} \sum_{J'=\frac{3}{2},\frac{5}{2}} -\Omega_{6P_J 5S} |6P_J\rangle\langle 5S| - \Omega_{6P_J 5D_{J'}} |6P_J\rangle\langle 5D_{J'}| + \text{H.c.}, \quad (1)$$

where $\Omega_{\alpha\beta}$ is the Rabi frequency between the two states labeled with α and β. It is defined by $\Omega_{\alpha\beta} = \mu_{\alpha\beta}\varepsilon/\hbar$, where $\mu_{\alpha\beta}$ and ε are the dipole moment and the electric field envelope. The time evolution of the atomic density operator $\hat{\rho}$ is given by

$$\frac{\partial \hat{\rho}}{\partial t} = -\frac{i}{\hbar}[\hat{V}(t), \hat{\rho}] - \sum_i \sum_j \Gamma_{ij}(1 - \delta_{ij})\rho_{ij}|i\rangle\langle j|, \quad (2)$$

where Γ is the dephasing rate resulting from the Doppler broadening effect. The initial state was assumed to be the coherent superposition created by the pump-pulse excitations. This approximation is valid as far as the pump-pulse duration is much shorter than the time evolution of YSF. We also assumed a swept inversion, with the pump pulse traveling through the medium at the speed of light without changing its shape. The spatiotemporal evolution of the radiation fields is given by

$$\frac{\partial \Omega_{\alpha\beta}}{\partial z} = i\eta_{\alpha\beta}\rho_{\alpha\beta}, \quad (3)$$

where $\eta_{\alpha\beta}$ is the coupling constant between the atomic polarization and the Rabi frequency and is calculated as $\eta_{\alpha\beta} = N\omega_{\alpha\beta}|\mu_{\alpha\beta}|^2/2c\epsilon_0\hbar$, where N, c, ϵ_0, and $\omega_{\alpha\beta}$ are the atomic number density, the speed of light, the vacuum permittivity, and the transition frequency between the two states labeled with α and β, respectively. The atomic number density was calculated from the pressure curve of Rb[20] and the cell temperature. By inserting the Hamiltonian from Eq. (1) into Eq. (2), we numerically solved the coupled differential equations of Eqs. (2) and (3) with the several assumptions mentioned below. To start with the temporal evolution of YSF, the constant Rabi frequencies, $\Omega_{6P_J 5D_{J'}}$, were introduced at $z = 0$ as a small phenomenological parameter [14,18]. We assumed that the lower transitions are Doppler broadened and substituted $\Gamma = 7 \times 10^{10}$ rad/s estimated from the relation $\Gamma = k\bar{c}_{rel}$, where k and $\bar{c}_{rel}$ are the wave number vector and the mean relative thermal velocity, respectively, for all terms between the $5S$ and $6P$ states, as well as between the $5S$ and $5D$ states.

V. SIMULATION RESULTS AND DISCUSSION

The simulated results of the squared Rabi frequency $|\Omega_{6P_{3/2}5S}|^2$, which is in proportion to the blue-light intensity, are shown in Fig. 4(a). The horizontal and vertical axes in the figure represent a peak intensity of the pump pulse and the time delay in the retarded frame with respect to the pump-pulse excitations, respectively. Because the $|\Omega_{6P_{1/2}5S}|^2$ is three orders of magnitude smaller than the $|\Omega_{6P_{3/2}5S}|^2$, its contribution to the blue light is assumed to be small and is not discussed here. The pump-pulse duration, the cell temperature, and the propagation length were up-chirped 300 fs, 170 °C, and 6 cm, respectively, which were similar to the experimental conditions. Due to the strong Rabi oscillations during the $5S - 5D$ two-photon absorption, the blue-light intensity showed a complex dependence on the pump-pulse intensity. A time integral of the squared Rabi frequency, $\int |\Omega_{6P_{3/2}5S}|^2 dt$, is shown in Fig. 4(b), and the oscillation is clearly exhibited. The above results can be compared with the experimental results. First, we retrieved the spatial profiles of the blue light. Considering that the pump beam is a Gaussian beam with a diameter of 1.23 mm, which is an average of the measured values, the peak intensity of the pump pulse was deduced from the measured pump-pulse power. For the pump-pulse power of A–D in Fig. 2(a), these values were estimated as 27 GW/cm^2, 67 GW/cm^2, 91 GW/cm^2, and 150 GW/cm^2, respectively. All of them were multiplied by a factor of 0.82 to reproduce the experimental results and indicated by A′-D′ in Fig. 4(b). These values were used to simulate the spatial profiles of the blue light, which are shown in the bottom row of Fig. 2(a). The simulated results well reproduced the experimental bright spots in A and C, as well as the characteristic ring-shaped profiles in B and D. In particular, the double-ring structure predicted from the simulation in B′ was clearly observed in B. Overall, the contrast was shaper in the experimental results than in the simulations. The agreement between the experimental and simulated results strongly supports our model, where the

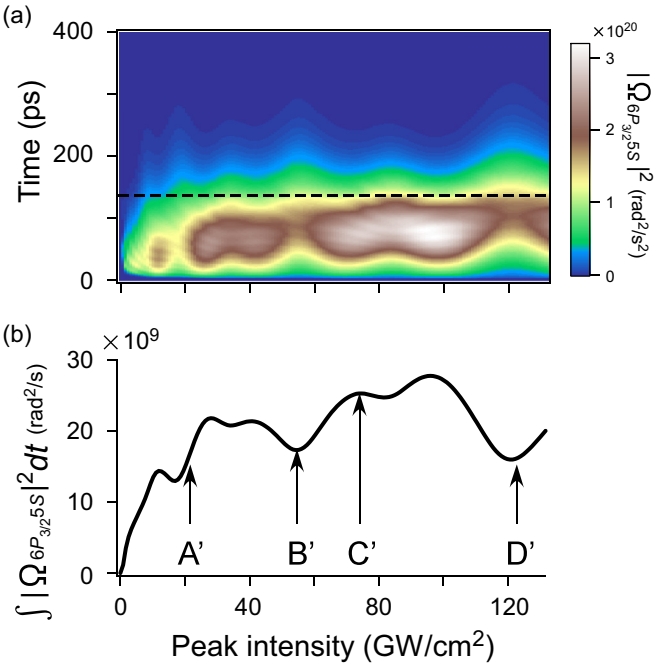

FIG. 4. (a) Two-dimensional plot of the squared Rabi frequency $|\Omega_{6P_{3/2}5S}|^2$ with respect to the time after the pump-pulse excitations (vertical axis) and the peak intensity of the pump pulse (horizontal axis). (b) Time-integrated squared Rabi frequency. The integration range, indicated by the dashed line in (a), is $0 - 135$ ps. A′-D′ indicate the intensities used in the simulations shown in the lower row in Fig. 2(a).

blue-light intensity is determined by the excitation process of individual atoms.

Next, we focused on the temporal profiles of the blue light. The simulated results at the pump-pulse intensity of 74 GW/cm^2, which is close to the value in C′, are shown in Fig. 3(b) for different temperatures in the range 170–200 °C. The simulated profiles were convolved with a Gaussian function with a 47-ps FWHM, which was derived from the fits of the reference pulses using a least-squares algorithm. The time origins of the experimental and simulated results were adjusted to each other so that the signals peak at the same time at 200 °C. Similar to the experimental results, the peak intensity of the blue light was larger and the relative delay to the pump pulse smaller at higher temperatures. The experimental peak at 170 °C was delayed ∼40 ps with respect to that at 200 °C, while the delay for the simulated one was 55 ps. In the experiment, the FWHMs of the blue-light pulses were ∼65 ps and ∼80 ps at 200 °C and 170 °C, respectively, which are close to the simulated values of 59 and 110 ps. On the other hand, the experimental peak intensity at 200 °C was enhanced by a factor of 30 with respect to that at 170 °C, which is three times larger than the enhancement factor of 9 in the simulations. Next, we estimated the blue-light power by using the energy flux calculated from Fig. 4(b) in combination with the experimental blue-light spatial profile of A in Fig. 2(b). The extrapolated FWHM of the blue light at the cell entrance is ∼94 μm in both horizontal and vertical directions. The roughly estimated blue-light power was ∼800 nW, which is one order of magnitude larger than the measured value of ∼90 nW. The several discrepancies between experiment and simulation results mentioned above might be due to a diffraction effect of the blue light or other decay processes from the initially excited $5D$ states, which were not included in the simulations.

Based on the quantitative agreement between the experimental and simulated results for both spatial and temporal characteristics of the blue light, we can then discuss in detail the time evolution of YSF, including the upper SF. The squared Rabi frequencies of the blue-light ($|\Omega_{6P_{3/2}5S}|^2$) and IR ($|\Omega_{6P_{3/2}5D_{5/2}}|^2$) emissions are plotted, on the left axis, as a function of time in Figs. 5(a) and 5(b), respectively. The pump-pulse parameters were the same as those in Fig. 3(b), while the temperature was fixed at 170 °C. The scale on the bottom axis in Fig. 5(b) is expanded with respect to that in Fig. 5(a). The squared Rabi frequencies of other upper transitions are three orders of magnitude smaller than the $|\Omega_{6P_{3/2}5D_{5/2}}|^2$, and hence are not discussed here. In Fig. 5(b), the first lobe of the IR emission peaks is at 4.5 ps, which is far sooner than the peak of the blue-light emission at around 100 ps in Fig. 5(a). The IR emission showed a strong temporal ringing due to the energy exchange between the field and the atoms. To clarify this, the populations of the atomic states are plotted on the right axis in Figs. 5(a) and 5(b). At the initial stage of YSF in Fig. 5(b), the IR field is developed, inducing the strong Rabi oscillation between $6P_{3/2}$ and $5D_{5/2}$ states. During the oscillation, the population of the $6P_{3/2}$ state is gradually transferred to the $5S$ state, resulting in the development of the blue-light field in Fig. 5(a).

In previous reports on YSF[12,14], the upper and lower fields were emitted almost simultaneously, which is in contrast to the behavior observed in Figs. 5(a) and 5(b). The difference

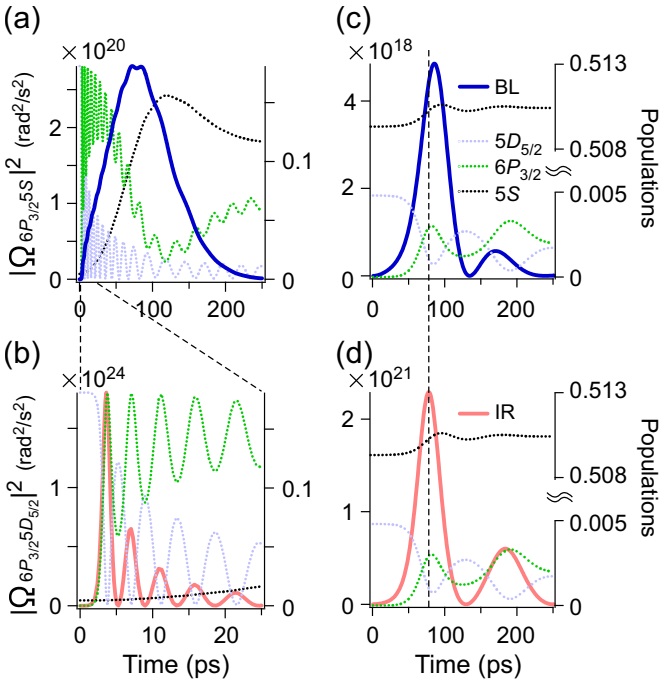

FIG. 5. Intensity of blue light (BL) (a) and IR (b) as well as atomic populations plotted as a function of the time delay with respect to the pump-pulse excitations. The pump-pulse parameters were the same as those in Fig. 3(b), while the temperature was fixed at 170 °C. Time evolution of the intensity of blue light (c) and IR (d) as well as the atomic populations at a pump-pulse peak intensity of 0.53 GW/cm^2 at 170 °C.

can be explained as follows. By differentiating Eq. (3) with respect to t and substituting Eq. (2) into the right side of the equation, the spatiotemporal evolution of the Rabi frequencies is given as

$$\frac{\partial^2\Omega_{6P5D}}{\partial z\partial t} = \frac{-\eta_{6P5D}}{\hbar} \times [\Omega_{6P5S}\rho_{5S5D} + \Omega_{6P5D}(\rho_{5D5D} - \rho_{6P6P})], \quad (4)$$

$$\frac{\partial^2\Omega_{6P5S}}{\partial z\partial t} = \frac{-\eta_{6P5S}}{\hbar} \times [\Omega_{6P5D}\rho_{5D5S} + \Omega_{6P5S}(\rho_{5S5S} - \rho_{6P6P})], \quad (5)$$

where the second term of the right side of Eq. (2) is neglected and the subscripts of $6P_{3/2}$ and $5D_{5/2}$ are omitted for simplicity. When the atomic populations are initially inverted ($\rho_{5D5D} \gg |\rho_{5S5D}|$) as in Figs. 5(a) and 5(b), the temporal evolution of the system is determined by the second term in the square brackets of Eqs. (4) and (5). Furthermore, as $|\eta_{6P5D}/\eta_{6P5S}| \sim 100$ for Rb atoms, the IR field develops sooner with respect to the blue-light field, explaining the results in Figs. 5(a) and 5(b). On the other hand, when the atomic populations are not inverted ($\rho_{5D5D} \ll |\rho_{5S5D}|$), the first term in the square brackets of Eqs. (4) and (5) might determine the temporal evolution of the system. By neglecting the second term of Eqs. (4) and (5),

we obtain

$$\frac{\partial^2 \Omega_{6P5D}}{\partial z \partial t} = \frac{-\sqrt{\eta_{6P5D}\eta_{6P5S}}}{\hbar} \Omega^*_{6P5D} \rho_{5S5D}, \tag{6}$$

$$\Omega^*_{6P5D} = \sqrt{\frac{\eta_{6P5D}}{\eta_{6P5S}}} \Omega_{6P5S}, \tag{7}$$

indicating that the blue-light and IR fields develop together. The above two cases are clearly distinguished by the parameter r defined in Ref. [11]:

$$r = \left| \frac{\eta_{6P5D}}{\eta_{6P5S}} \frac{\rho_{5D5D}}{\rho_{5S5S}} \right| \simeq 100 \frac{\rho_{5D5D}}{\rho_{5S5S}}. \tag{8}$$

In the case of $r > 1$ and $r < 1$, the system is defined strongly and weakly excited, respectively. In our results in Figs. 5(a) and 5(b), $r \sim 3400$. For comparison, we simulated the time evolution of YSF in the weak excitation regime, in which a pump pulse with a peak intensity of 0.53 GW/cm^2 is applied, resulting in $r \sim 0.9$. Figures 5(c) and 5(d) show blue-light and IR fields as functions of time on the left axis as well as the atomic populations on the right axis. As expected, the temporal profiles of blue-light and IR pulses were almost same and the atoms relaxed from the initially populated $5D_{5/2}$ state to the $5S$ one via the intermediate $6P_{3/2}$ state during the emissions. This behavior is close to the YSF observed so far. In Ref. [14] the experiment was performed in the same system as ours with the pump-pulse intensity below the blue-light saturation. In Ref. [12] the YSF was observed on the $6D_{3/2} - 6P_{1/2}$ and $6P_{1/2} - 6S_{1/2}$ transitions of Cs atoms with $|\eta_{6P6D}/\eta_{6P6S}| < 1$, which is much smaller than $|\eta_{6P5D}/\eta_{6P5S}| \sim 100$ of Rb atoms. These experiments are assumed to be conducted in the weak excitation regime; therefore, they are consistent with our results.

The YSF dynamics discussed in this paper is different from that treated in the previous reports. The two emission fields were cascaded rather than yoked. Nevertheless, the beam divergence results given in Fig. 2(b) still support the production of the blue light via a time-delayed FWM process even in the strong excitation regime. Therefore, the blue-light emission observed in our experiment is essentially different from the traditional cascade SF[2] considering the crucial role of the coherence between ground and excited states.

VI. CONCLUSION

We investigated the spatiotemporal profiles of the YSF emitted from a dense atomic Rb vapor by driving the $5S - 5D$ two-photon transition in the strong excitation regime with an ultrashort laser pulse. By increasing of the pump-pulse power, the shape of the emitted blue light periodically changed between a bright spot and a ring-shaped radial profile. The bright spot propagated as a low-divergence beam with a divergence angle consistent with that predicted from the FWM process. The temporal profile of the blue light was recorded with a time resolution of $\sim$50 ps. The experimental spatial and temporal profiles were reproduced by simulations using the Maxwell-Bloch equations. The simulated results revealed that, in the strong excitation regime, the development of the lower field is significantly delayed with respect to that of the upper field, which is in contrast with the behavior in the weak excitation regime, where the two emission fields are temporally overlapped. Nevertheless, our beam divergence analysis still supports the theory that the blue light is produced via a time-delayed FWM process even in the strong excitation regime.

Although we focused on the intensity of the blue light throughout this paper, its phase should be investigated as well. In the strong excitation regime, the nonlinear atomic response might modulate the local phase of the blue light depending on the local intensity of the pump field, resulting in a spatially nonuniform phase of the blue-light field. In this sense, a focusing property of the blue light would be of great interest [24].

ACKNOWLEDGMENTS

We thank Dr. Y. Miyamoto for useful discussions. This work was financially supported by JSPS KAKENHI Grant No. 18K04984.

[1] R. H. Dicke, Phys. Rev. **93**, 99 (1954).
[2] M. S. Feld and J. C. MacGillivray, *Coherent Nonlinear Optics, Superradiance* (Springer-Verlag, Berlin, 1980).
[3] F. P. Matter, H. M. Gibbs, S. L. McCall, and M. S. Feld, Phys. Rev. Lett. **46**, 1123 (1981).
[4] N. Skribanowitz, I. P. Herman, J. C. MacGillivray, and M. S. Feld, Phys. Rev. Lett. **30**, 309 (1973); H. M. Gibbs, Q. H. F. Vrehen, and H. M. J. Hikspoors, *ibid.* **39**, 547 (1977).
[5] M. S. Malcuit, J. J. Maki, D. J. Simkin, and R. W. Boyd, Phys. Rev. Lett. **59**, 1189 (1987).
[6] M. Nagasono, J. R. Harries, H. Iwayama, T. Togashi, K. Tono, M. Yabashi, Y. Senba, H. Ohashi, T. Ishikawa, and E. Shigemasa, Phys. Rev. Lett. **107**, 193603 (2011).
[7] G. T. Noe II, Ji-Hee Kim, J. Lee, Y. Wang, A. K. Wójcik, S. A. McGill, D. H. Reitze, A. A. Belyanin, and J. Kono, Nat. Phys. **8**, 219 (2012).
[8] C. R. Ding, W. Lin, B. C. Chen, F. L. Zhao, J. W. Dong, M. Shi, H. Z. Wang, Y. F. Hsu, and A. B. Djurišić, Appl. Phys. Lett. **93**, 151902 (2008).
[9] A. I. Chumakov *et al.*, Nat. Phys. **14**, 261 (2017).
[10] J. C. MacGillivray and M. S. Feld, Phys. Rev. A **14**, 1169 (1976); D. Polder, M. F. H. Schuurmans, and Q. H. F. Vrehen, *ibid.* **19**, 1192 (1979).
[11] K. Ikeda, J. Okada, and M. Matsuoka, J. Phys. Soc. Jpn. **48**, 1636 (1980).
[12] J. H. Brownell, X. Lu, and S. R. Hartmann, Phys. Rev. Lett. **75**, 3265 (1995).
[13] A. I. Lvovsky, S. R. Hartmann, and F. Moshary, Phys. Rev. Lett. **82**, 4420 (1999); A. I. Lvovsky, Ph.D. thesis, Columbia University, 1998.
[14] G. O. Ariunbold, M. M. Kash, V. A. Sautenkov, H. Li, Y. V. Rostovtsev, G. R. Welch, and M. O. Scully, Phys. Rev. A **82**, 043421 (2010).

[15] B. Gai, S. Hu, J. Liu, R. Cao, J. Guo, Y. Jin, and F. Sang, Opt. Commun. **374**, 142 (2016); Z. Yi, P. K. Jha, L. Yuan, D. V. Voronine, G. O. Ariunbold, A. M. Sinyukov, Z. Di, V. A. Sautenkov, Y. V. Rostovtsev, and A. V. Sokolov, *ibid.* **351**, 45 (2015); G. O. Ariunbold, V. A. Sautenkov, and M. O. Scully, Opt. Lett. **37**, 2400 (2012); C. V. Sulham, G. A. Pitz, and G. P. Perram, Appl. Phys. B **101**, 57 (2010); G. O. Ariunbold, M. M. Kash, V. A. Sautenkov, H. Li, Y. V. Rostovtsev, G. R. Welch, and M. O. Scully, J. Opt. Soc. Am. B **28**, 515 (2011); D. Felinto, L. H. Acioli, and S. S. Vianna, Opt. Lett. **25**, 917 (2000).

[16] G. O. Ariunbold, V. A. Sautenkov, Y. V. Rostovtsev, and M. O. Scully, Appl. Phys. Lett. **104**, 021114 (2014); A. Dogariu, J. B. Michael, M. O. Scully, and R. B. Miles, Science **331**, 442 (2011).

[17] K. Kitano and H. Maeda, Opt. Express **25**, 23826 (2017).

[18] L. Yuan, B. H. Hokr, A. J. Traverso, D. V. Voronine, Y. Rostovtsev, A. V. Sokolov, and M. O. Scully, Phys. Rev. A **87**, 023826 (2013).

[19] E. Paradis, B. Barrett, A. Kumarakrishnan, R. Zhang, and G. Raithel, Phys. Rev. A **77**, 043419 (2008).

[20] P. Siddons, C. S. Adams, C. Ge, and I. G. Hughes, J. Phys. B **41**, 155004 (2008).

[21] R. N. Zare, *Angular Momentum* (Wiley-Interscience, New York, 1986).

[22] M. S. Safronova, C. J. Williams, and C. W. Clark, Phys. Rev. A **69**, 022509 (2004).

[23] J. T. Manassah and B. Gross, Opt. Commun. **119**, 663 (1995).

[24] R. Dorn, S. Quabis, and G. Leuchs, Phys. Rev. Lett. **91**, 233901 (2003).